Essential Topics in Materials Physics and Chemistry

Volume III

Heather Dale

Essential Topics in Materials Physics and Chemistry

Volume III

Edited by **Heather Dale**

NY RESEARCH PRESS
New York

Published by NY Research Press,
23 West, 55th Street, Suite 816,
New York, NY 10019, USA
www.nyresearchpress.com

Essential Topics in Materials Physics and Chemistry: Volume III
Edited by Heather Dale

International Standard Book Number: 978-1-63238-189-7 (Hardback)

Printed in China.

Essential Topics in Materials Physics and Chemistry

Volume III

Preface

Our understanding of the world is rapidly evolving as scientific methods go deeper and deeper into unraveling the universe. Basic physical science fields have also evolved, changed and advanced accordingly and the fields of materials Physics and Chemistry have gained a foothold. The discipline that focuses on the relationship between the atoms, molecules or ions that constitute a material and its overall physical characteristics is called Materials Chemistry. In this field, the material and structure of materials is studied as well as synthesizing new materials. What is surprising is the fact that until perhaps 20 years ago the words 'materials' and 'chemistry' were hardly used together. Advanced technological progress has also been helpful in using computational techniques to predict the material and structure of still undiscovered matter. On the other hand Material physics is instrumental in describing materials in terms of mechanics, heat, light and force. It combines sciences such as chemistry and solid state physics along with solid mechanics. Like materials chemistry has a bit of chemistry in its methodology, so too has physics got chemistry. In recent years such materials sciences have reached a respected and secure place in the scientific community.

This book lists and discusses the research compiled on the advances that materials physics and chemistry have had recently. I am thankful to those scientists and researchers whose toil and hard work help make this book a success as well as those outside the scientific community who have been unwavering in their support

Editor

Contents

	Preface	**XI**
Chapter 1	**Impacts of Melt Spinning and Element Substitution on Electrochemical Characteristics of the La-Mg-Ni-based A_2B_7-Type Alloys** Yang-huan Zhang, Hong-wei Shang, Ying Cai, Zhong-hui Hou, Guo-fang Zhang, Dong-liang Zhao	**1**
Chapter 2	**Thermal Degradation Kinetics of iPP/Pd Nanocomposite Prepared by a Drying Process** Y Jae-Young Lee, Hong-Ki Lee, Sung-Wan Hong, Il-Yub Choi	**7**
Chapter 3	**Fabrication of Sn Coatings on Alumina Balls by Mechanical Coating Technique and Relevant Process Analysis** Liang Hao, Yun Lu, Hiromasa Sato, Kazuki Chiba	**12**
Chapter 4	**Jet Plasma-Chemical Reactor for the Conversion of Methane: the Use of Clustering** A. E. Zarvin, N. G. Korobeishchikov, M. D. Khodakov, V. V. Kalyada	**16**
Chapter 5	**Hydrogen as Carbon Gasifying Agent During Glycerol Steam Reforming over Bimetallic Co-Ni Catalyst** Chin Kui Cheng, Rwi Hau Lim, Anabil Ubil, Sim Yee Chin, Jolius Gimbun	**20**
Chapter 6	**Simulation of Countercurrent Multi-Effect Drying System** Hong Li, Lianying Wu, Xianli Wu, Yangdong Hu	**24**
Chapter 7	**Synthesis of Aluminum-doped Zinc Oxide Nanowires Hydrothermally Grown on Plastic Substrate** Concepción Mejía García, Elvia Díaz Valdés, Ana Ma. Paniagua Mercado, Arturo F. Méndez Sánchez, José A. Andraca Adame, Velumani Subramaniam, Josué Romero Ibarra	**30**
Chapter 8	**Antibacterial Activity of TiO_2/Ti Composite Photocatalyst Films Treated by Ultrasonic Cleaning** Yun Lu, Lian Hao, Yutaka Hirakawa, Hiromasa Sato	**34**
Chapter 9	**Fluoride Processing of Titanium-Containing Minerals** N. M. Laptash, I. G. Maslennikova	**38**

Chapter 10 **Laser Deposition of Tetrasulfonated Phthalocyanine Layers for Gas Sensors** 42
Premysl Fitl, Martin Vrnata, Dusan Kopecky, Jan Vlcek, Jitka Skodova, Jaroslav Hofmann, Vladimir Myslik

Chapter 11 **Biodiesel Production from Rubber Seed Oil Using A Limestone Based Catalyst** 47
Jolius Gimbun, Shahid Ali, Chitra Charan Suri Charan Kanwal, Liyana Amer Shah, Nurul Hidayah Muhamad Ghazali, Chin Kui Cheng, Said Nurdin

Chapter 12 **Optimization of Draft Tube Position in a Spouted Bed Reactor using Response Surface Methodology** 51
Elaheh Baghban, Arjomand Mehrabani-Zeinabad

Chapter 13 **Resolving a Challenge in the Modeling of Hydrogen Production Using Steam Reforming of Methane in Monolith Reactors Using CFD Methods** 55
Mohammad Irani

Chapter 14 **BPSCCO Superconducting Films Grown by Spray Pyrolysis Technique: Systematic Study of the Relationship between Pb Content and Annealing Conditions** 60
Y Elvia Díaz Valdés, Concepción Mejía García, Ana María Paniagua Mercado, Arturo Méndez Sánchez

Chapter 15 **Adsorption of Cu(II), Ni(II), Zn(II), Cd(II) and Pb(II) onto Kaolin/Zeolite Based- Geopolymers** 64
Bassam El-Eswed, Mazen Alshaaer, Rushdi Ibrahim Yousef, Imad Hamadneh, Fawwaz Khalili

Chapter 16 **Aqueous Two Phase Extraction for the Recovery of 1,3-Propanediol from Its Aqueous Solutions** 71
Min Hee Chung, Yeon Ki Hong, Hyoung Wook Lee, Sung-Jun Park

Chapter 17 **Research of Extent of Well Control of Explored Reserves of Lithologic Deposit in Delta Front Area** 75
Ma Dong

Chapter 18 **The Study of Method for Complex Processing Turgay Sub-Standard Aluminum-Containing Raw Materials** 79
G. Sarsenbay, L. A. Myltykbaeva, R. A. Abdulwalyev, S. B. Satylganova

Chapter 19 **Experimental Studies on the Influence of HCO_3^- on Absorption and Desorption of CO_2 from Ammonia Solution** 84
Shaojian Jiang, Wei Zhong, Rui Peng, Yong Jiang, Jun Zhang

Chapter 20 **Catalytic Feedstock Recycling of Polymers A Green Approach Towards Sustainable Environment** 88
Raju Francis, Beena Sethi

Chapter 21 **Synthesis and Electrochemical Characterization of Li_2MnSiO_4 with Different Crystal Structure as Cathode Material in Lithium Rechargeable Batteries** 92
Joongpyo Shim, Sora Won, Gyungse Park, Ho-Jung Sun

Chapter 22 **Preparation and Property Analysis of Melamine Formaldehyde Foam** 96
Dongwei Wang, Xiaoxian Zhang, Song Luo, Sai Li

Chapter 23 **A First-Principles Study of Structure-Property Correlation and the Origin of Ferrimagnetism in Gallium Ferrite** 101
Amritendu Roy, Ashish Garg, Rajendra Prasad, Sushil Auluck

Chapter 24 **Low Temperature Electrical Transport in Double Layered CMR Manganite $La_{1.2}Sr_{1.4}Ba_{0.4}Mn_2O_7$** 105
Y. S. Reddy, P. Kistaiah, C. Vishnuvardhan Reddy

Chapter 25 **Preparation of High Ga Content Cu(In,Ga)Se_2 Thin Films by Sequential Evaporation Process Added In_2S_3** 109
Toshiyuki Yamaguchi, Kazuma Tsujita,
Shigetoshi Niiyama, Toshito Imanishi

Chapter 26 **Research on Supercritical Methanol Treatment of Lignite** 113
Haiyan Luan, Aiguo Wang, Qian Zhang, Fuming Chen

Chapter 27 **Simulation of Multi-stage Flash (MSF) Desalination Process** 117
Lian-ying Wu, Sheng-nan Xiao, Cong-jie Gao

Chapter 28 **In Vitro Study of Carbamate-Linked Cationic Lipid for Gene Delivery Against Cervical Cancer Cells** 123
Defu Zhi, Shuibao Zhang, Yinan Zhao, Shaohui Cui, Bing Wang,
Huiying Chen, Defu Zhi, Defeng Zhao

Chapter 29 **Simulation of Thermophysical Processes at Laser Welding of Alloys Containing Refractory Nanoparticles** 127
Anatoly N. Cherepanov, Vasily P. Shapeev, Guangxun Liu, Lamei Cao

Chapter 30 **Mixing Enhancement in a Coaxial Jet Mixer** 131
Valery Zhdanov, Egon Hassel

Chapter 31 **Investigation of the Surface Properties of Vinyl Ethers - Sodium 2-Acrylamido-2-Methylpropanesulfonate Copolymers** 135
S. Kh. Khussain, E. M. Shaikhutdinov, N. Zh. Seitkaliyeva,
A. Zh. Zhenisova

Chapter 32 **Preparation, Characterization and Thermal Expansion of Pr Co-Dopant in Samarium Doped Ceria** 139
V. Venkatesh, V. Prashanth Kumar, R. Sayanna,
C. Vishnuvardhan Reddy

Chapter 33 **Sustainable Polymers Derived From Naturally Occurring Materials** 143
Bimlesh Lochab, I. K. Varma, J. Bijwe

Chapter 34 **Pulsed Gas Jets for Formation of High-Intensity Cluster Beams** 148
N. G. Korobeishchikov, A. E. Zarvin, V. V. Kalyada, A. A. Schmakov

Chapter 35 **Coacervation Microencapsulation of $CaCO_3$ Particles with a Fluoropolymer by Pressure-Induced Phase Separation of Supercritical Carbon Dioxide Solutions** 152
Kenji Mishima, Haruo Yokota, Takafumi Kato, Tadashi Suetsugu, Xiuqin Wei, Keiichi Irie, Kenichi Mishima, Michihiro Fujiwara

Chapter 36 **Influence of Waste Materials Containing Tungsten on Melting and Crystallization of Glass-ceramics** 156
Shaomin Lin, Bo Wang, Guishen Liu, Liqing Li, Xiaodong Hou

Chapter 37 **Evaluation of UV Optical Fibers Behavior under Neutron Irradiation** 160
Dan Sporea, Adelina Sporea, Mirela Ancuta, Dumitru Barbos, Maria Mihalache, Mirea Mladin

Chapter 38 **Developing a Mathematical Model for Hydrate Formation in a Spray Batch Reactor** 164
Mohammad Kazemeini, Farideh Freidoonian, Moslem Fattahi

Chapter 39 **Photocatalytic of TiO_2-SiO_2 Thin Films Co-Doped with Fe^{3+} and Thio-Urea in the Degradation of Formaldehyde by Indoor and Outdoor Visible Lights** 168
Charuwan Kaewtip, Kamolporn Accanit, Nat-a-nong Chaowai, Kanokpun Areerat, Pasuree Reanjaruan, Virote Boonumnauyvitaya

Chapter 40 **Sol-Gel Synthesis of TiO_2 Thin Films from In-House Nano-TiO_2 Powder** 173
Mohd Zainizan Sahdan, Nafarizal Nayan, Samsul Haimi Dahlan, Mahdi Ezwan Mahmoud, Uda Hashim

Chapter 41 **Micromixing of a Two Phase System in a Stirred Tank with Multiple Impellers** 178
Lei Yang, Jingcai Cheng, Ping Fan, Chao Yang

Chapter 42 **Yttria Promoted Nickel Nanowire Catalyst for the Partial Oxidation of Methane to Synthesis Gas** 182
Xuebin Hong, Bingbing Li, Cong Zhang

Chapter 43 **Progress of Modern Pyrolysis Furnace Technology** 186
Guotai Zhang, Bruce Evans

Chapter 44 **Influence of Humidity on Yield Stress Determination by Slump Test of Slip-Prone Clayey Soils and Their Relation with the Chemical Properties** 190
Arturo F. Méndez-Sánchez, Ana M. Paniagua-Mercado, Karen E. Nieto-Zepeda, Leonor Pérez-Trejo, Elvia Diaz Valdés, Concepción Mejía García

Chapter 45 **Apatite Deposition on ZrO_2 Thin Films by DC Unbalanced Magnetron Sputtering** 194
Arisara Thaveedeetrakul, Virote Boonamnuayvitaya, Nirun Witit-anun

Permissions

List of Contributors

Impacts of Melt Spinning and Element Substitution on Electrochemical Characteristics of the La–Mg–Ni-based A_2B_7-Type Alloys

Yang-huan Zhang[1,2], Hong-wei Shang[1,2], Ying Cai[1], Zhong-hui Hou[1], Guo-fang Zhang[1,2], Dong-liang Zhao[2]
[1]Key Laboratory of Integrated Exploitation of Baiyun Obo Multi-Metal Resources,
Inner Mongolia University of Science and Technology Baotou, China
[2]Department of Functional Material Research, Central Iron and Steel Research Institute, Beijing, China

ABSTRACT

The partial substitution of Zr for La has been performed in order to ameliorate the electrochemical hydrogen storage performances of La–Mg–Ni based A_2B_7-type electrode alloys. The melt spinning technology was used to prepare the $La_{0.75-x}Zr_xMg_{0.25}Ni_{3.2}Co_{0.2}Al_{0.1}$ (x=0, 0.05, 0.1, 0.15, 0.2) electrode alloys. The impacts of the melt spinning and the substituting La with Zr on the structures and the electrochemical hydrogen storage characteristics of the alloys were systemically investigated. The analysis of XRD and TEM reveals that the as-cast and spun alloys have a multiphase structure, composing of two main phases $(La, Mg)_2Ni_7$ and $LaNi_5$ as well as a residual phase $LaNi_2$. The electrochemical measurement indicates that both the substitution of Zr for La and the melt spinning ameliorate the electrochemical cycle stability of the alloys dramatically. Furthermore, the high rate discharge ability (HRD) of the as-spun (10 m/s) alloys notably declines with growing the amount of Zr substitution, while it first augments and then falls for the (x=0.1) alloy with rising the spinning rate.

Keywords: A_2B_7-Type Alloy; Substituting La with Zr; Melt-Spinning; Electrochemical Characteristics

1. Introduction

With rapid development of electric equipments, the requirement for new electrode materials with superior performances, especially high discharge capacity and electrochemical hydrogen storage kinetics, has become more and more pressing. The rare earth-based AB_5-type alloys, although have been industrialized in large scale in China and Japan, are suffering a severe frustration on account of their limited discharge capacity of about 330 mAh/g. La–Mg–Ni-system AB_3 and A_2B_7-type alloys have been considered to be the most promising candidates as the negative electrode materials of Ni–MH rechargeable battery in virtue of their higher discharge capacities (380–410 mAh/g) and low production costs since Kadir et al. [1] and Kohno et al. [2] reported their research results. The National High Technology Research and Development Program of China (for short "863" Program) provides powerful financial support in order to promote the industrialization of these new-type alloys. Such a lot of efforts have been dedicated to realizing this target and dramatic progress has been achieved, about which Liu et al. have published a perfect summarization recently [3,4]. However, the Chinese researchers in this area were deeply frustrated by a fact that the production of the new type alloys as the negative electrode in Ni–MH battery has not been found in China as a result of little poor electrochemical cycle stability of the electrode alloys. A serious challenge faced by researchers keeps intact, enhancing the cycle stability of the alloy without reducing its discharge capacity.

The element substitution has been regarded as one of the effective methods for improving the overall properties of the hydrogen storage alloys. In addition, the preparation technology is also extremely important for improving the performances of the alloys. Therefore, it is expected that the combination of an optimized amount of Zr substitution with a proper melt spinning technique may yield an alloy with high discharge capacity and good cycling stability. The A_2B_7-type $La_{0.75-x}Zr_xMg_{0.25}Ni_{3.2}Co_{0.2}Al_{0.1}$ (x=0-0.2) alloys were prepared by melt spinning, and a systematic investigation on the effects of the substitution of Zr for La and the melt spinning on the electrochemical cycle stability and kinetics of the electrode alloys has been performed.

2. Experimental

The chemical compositions of the alloys were $La_{0.75-x}Zr_xMg_{0.25}Ni_{3.2}Co_{0.2}Al_{0.1}$ (x=0, 0.05, 0.1, 0.15, 0.2). For convenience, the alloys were denoted with Zr content as Zr_0, $Zr_{0.05}$, $Zr_{0.1}$, $Zr_{0.15}$ and $Zr_{0.2}$, respectively. The alloy ingots were prepared using a vacuum induction furnace in a helium atmosphere under a pressure of 0.04 MPa. A part of the as-cast alloys was re-melted and spun by melt-spinning with a rotating copper roller. The spinning rate was approximately expressed by the linear velocity of the copper roller. The spinning rates used in the experiment were 5, 10, 15 and 20 m/s, respectively.

The phase structures and compositions of the as-cast and

*Supported by National Natural Science Foundations of China (51161015 and 50961009), National 863 plans projects of China (2011AA03A408), Natural Science Foundation of Inner Mongolia, China (2011ZD10 and 2010ZD05).

spun alloys were characterized by XRD (D/max/2400). The thin film samples of the as-spun alloys were prepared by ion etching for observing the morphology with HRTEM (JEM-2100F).

The round electrode pellets in a 15 mm diameter were prepared by cold pressing a mixture of alloy powder and carbonyl nickel powder in the weight ratio of 1:4 under a 35 MPa pressure. After dried for 4 h, the electrode pellets were immersed in a 6 M KOH solution for 24 h in order to wet the electrodes fully before the electrochemical measurement.

Electrochemical measurements were performed at 30°C by using a tri-electrode open cell, consisting of a working electrode (the metal hydride electrode), a sintered $Ni(OH)_2/NiOOH$ counter electrode and a Hg/HgO reference electrode, which were immersed in a 6M KOH electrolyte. The voltage between the negative electrode and the reference electrode was defined as the discharge voltage. In every cycle, the alloy electrode was firstly charged with a constant current density of 300 mA/g. After resting 15 min, it was discharged at the same current density to cut-off voltage of –0.500 V.

The electrochemical impedance spectra (EIS), the hydrogen diffusion in alloy bulk and the Tafel polarization curves of the alloys were measured by an electrochemical workstation (PARSTAT 2273). The EIS of the alloy electrodes were measured in the frequency range from 10 kHz to 5 mHz at 50% depth of discharge (DOD). The Tafel polarization curves were measured in the potential range of –1.2 to +1.0 V (vs. Hg/HgO) with a scan rate of 5 mV/s also at 50% depth of discharge. For the potentiostatic discharge, the test electrodes in the fully charged state were discharged at 500 mV potential steps for 5000s, using the electrochemistry corrosion software (Corr-Ware).

3. Results and Discussion

3.1. Structural characteristics

The XRD patterns of the as-cast and spun $La_{0.75-x}Zr_xMg_{0.25}Ni_{3.2}Co_{0.2}Al_{0.1}$ (x=0-0.2) alloys are presented in **Figure 1**. It is evident that the melt spinning and Zr substitution bring on an obvious broadening of the major diffraction peaks of the alloys, to be ascribed to the refined grain and the stored stress in the grains by melt spinning and Zr substitution. It is found that the as-cast and spun alloys hold a multiphase structure, composing of two major phases $(La, Mg)_2Ni_7$ and $LaNi_5$ as well as a residual phase $LaNi_2$. The structures of the alloys maintain almost unaltered after partially substituted by Zr. The lattice parameters together with the abundances of the $(La, Mg)_2Ni_7$ and $LaNi_5$ major phases in the alloys, which were calculated by Jade 6.0 software based on the XRD data, are listed in **Table 1**. It is found that the Zr substitution arouses an increase of the $LaNi_5$ phase and a decrease of the $(La, Mg)_2Ni_7$ phase. Meanwhile, it also leads to a decrease of the lattice constants and cell volume of the two major phases, which is due to the fact that the atom radius of Zr is smaller than that of La. Furthermore, the shrink of the cell volume, incurred by the substitution, justifies the successful alloying of Zr with $(La, Mg)_2Ni_7$ and $LaNi_5$ major phases.

The TEM micrographs of the as-spun (10 m/s) $La_{0.75-x}Zr_xMg_{0.25}Ni_{3.2}Co_{0.2}Al_{0.1}$ (x=0-0.2) alloys are demonstrated in **Figure 2**. It can be seen from **Figure 2** that the change of the morphologies of the alloys seems to be equivocal with the various of Zr content. However, the amplified morphologies of **Figure 2** reveal that the as-spun Zr_0 and $Zr_{0.1}$ alloys display an entire crystalline structure. And some crystal defects such as subgrains and grain boundaries can be seen clearly. It is evident that $Zr_{0.2}$ alloy displays an obvious amorphous-like structure, and the nanocrystalline region, the amorphous region as well as the transition region can be clearly viewed from the amplified morphology of **Figure 2(c)**, which seems to be conflicting with the result in **Figure 1** due to no amorphous phase is detected by XRD observation. One probable reason is that the amorphous-like phase forms at some selective locations in the as-spun alloy and its amount is very small, thus, the XRD patterns could not detect its presence.

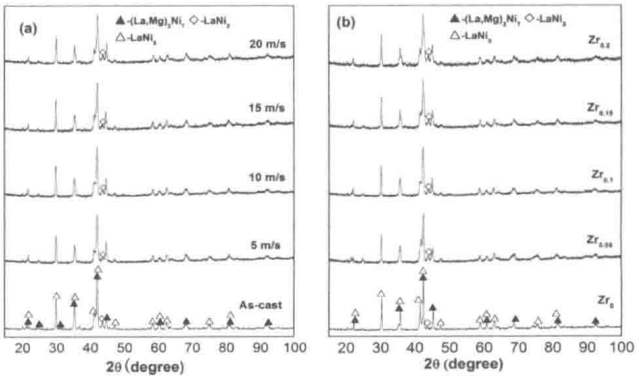

Figure 1. XRD profiles of the as-cast spun alloys: (a) $Zr_{0.1}$, (b) As-spun (10 m/s)

Table 1. Lattice parameters, abundances of $LaNi_5$ and $(La, Mg)_2Ni_7$ major phases.

Spinning rate	Alloys	Major phases	Lattice constants		Cell volume	Phase abund-ance
			A(nm)	*C(nm)*	*V (nm^3)*	*(wt.%)*
10 m/s	Zr_0	$(La, Mg)_2Ni_7$	0.5199	2.4406	0.5712	72.31
		$LaNi_5$	0.5192	0.4180	0.0976	25.24
	$Zr_{0.05}$	$(La, Mg)_2Ni_7$	0.5142	2.4362	0.5578	66.03
		$LaNi_5$	0.5130	0.4107	0.0936	31.02
	$Zr_{0.1}$	$(La, Mg)_2Ni_7$	0.5071	2.4308	0.5413	64.25
		$LaNi_5$	0.5059	0.4082	0.0905	34.08
	$Zr_{0.15}$	$(La, Mg)_2Ni_7$	0.5031	2.4251	0.5315	60.97
		$LaNi_5$	0.5011	0.4053	0.0881	36.50
	$Zr_{0.2}$	$(La, Mg)_2Ni_7$	0.4963	2.4174	0.5156	58.02
		$LaNi_5$	0.4933	0.4021	0.0847	39.32

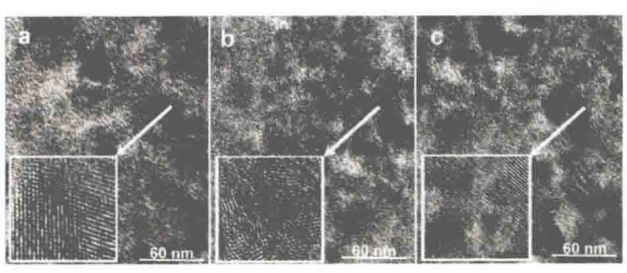

Figure 2. TEM micrographs of the as-spun (10 m/s) alloys: (a) Zr_0 alloy, (b) $Zr_{0.1}$ alloy, (c) $Zr_{0.2}$ alloy.

3.2. Electrochemical Cycle Stability and Kinetics

The capacity retaining rate (R_N) is introduced as a token of the electrochemical cycle stability of an alloy electrode, which is defined as $R_N = C_N/C_{max} \times 100\%$, where C_{max} is the maximum discharge capacity while C_N is the discharge capacity at the nth charging–discharging cycle with a current density of 300 mA/g, respectively. The evolution of the capacity retaining rates (R_N) of the $La_{0.75-x}Zr_xMg_{0.25}Ni_{3.2}Co_{0.2}Al_{0.1}$ (x=0-0.2) alloys with the cycle number is described in **Figure 3**. The slopes of the curves in **Figure 3** prefigure the degradation rate of the discharge capacity during the charge-discharge cycling. The smaller the slope of the curve is, the better the cycle stability of the alloy will be. It is evident that the degradation rate of the discharge capacity of the alloys visibly declines with rising the spinning rate and the Zr content. In order to establish the relationship between the capacity retaining rates (R_N) with the spinning rate and the Zr content, taking the capacity retaining rate (R_{100}) at 100th cycling as a benchmark, the evolution of the R_{100} of the alloys with the spinning rate and the amount of Zr substitution is also inserted in **Figure 3**. It is found that the R_{100} values of the alloys markedly augment with growing the spinning rate and the Zr content. The R_{100} value of the $Zr_{0.1}$ alloy grows from 73.21% to 82.07% as the spinning rate increases from 0 (as-cast was defined as the spinning rate of 0 m/s) to 20 m/s and that of the as-spun (10 m/s) alloys augments from 69.25% to 83.09% as Zr content rises from 0 to 0.2.

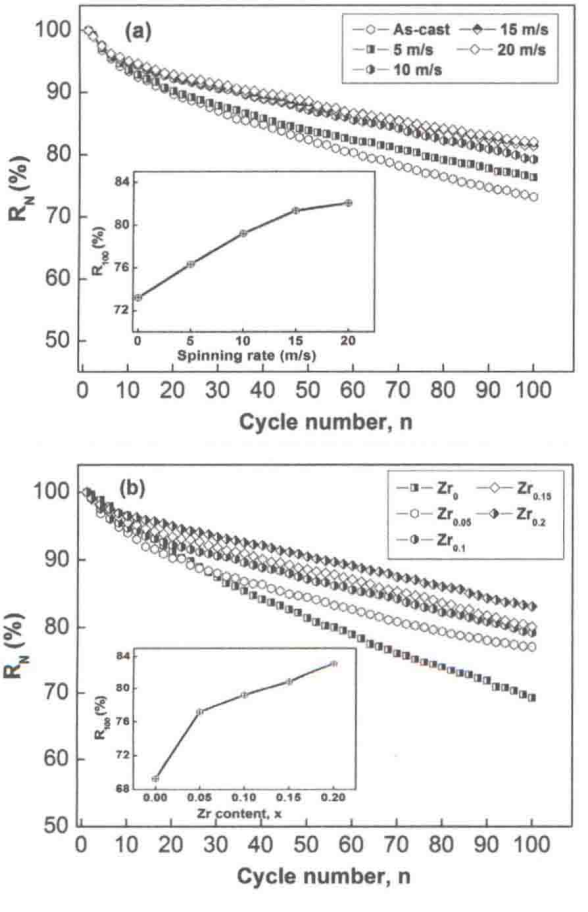

Figure 3. Evolution of the capacity retaining rates (R_N) of the alloys with the cycle number: (a) $Zr_{0.1}$ alloy, (b) As-spun (10 m/s).

It is convinced that the pulverization and oxidation of the alloy during charging-discharging cycle are the fundamental reason for the capacity decay of the electrode alloy. The lattice stress and the expansion of the cell volume, which are inevitable when hydrogen atoms entering into the interstitials of the lattice, are the real driving force lead to the pulverization and oxidation. The positive impact of the melt spinning on the cycle stability of the alloy is primarily ascribed to the remarkable refinement of the grains induced by melt spinning. The anti-pulverization capability of the alloy basically depends on its grain size. Therefore, it is understandable that the cycle stability of the alloy increases with growing the spinning rate. The benefaction of the Zr substitution on the cycle stability of the as-spun alloys is primarily ascribed to the formation of an amorphous phase induced by the melt spinning due to an amorphous phase improves not only anti-pulverization ability but also anti-corrosion and anti-oxidation abilities of the alloy electrode in a corrosive electrolyte [5].

The electrochemical hydrogen storage kinetics of an alloy electrode, which has been considered to be quite important for the practical application of hydride electrode in power battery, is symbolized by its high rate discharge ability (HRD), being calculated by formula: $HRD=C_i/C_{100} \times 100\%$, where C_i and C_{100} are the maximum discharge capacities of the alloy electrode charged-discharged at the current densities of i and 100 mA/g respectively. The current density dependence of the HRD values of the alloys is illustrated in **Figure 4**. In order to establish the relationship between the electrochemical hydrogen storage kinetics of the alloys with the spinning rate and the amount of Zr substitution, taking the 900 mA/g current density as a benchmark to calculate the HRD of the alloys, the evolution of the HRD (i=900 mA/g) of the alloys with the spinning rate and the Zr content is also inset in **Figure 4**. It is evident that the melt spinning gives rise to a slight increase in the HRD of $Zr_{0.1}$ alloy as the spinning rate grows from 0 to 5 m/s, but with further increase of the spinning rate, it brings on a dramatic decline of the HRD. The HRD of the as-spun (10 m/s) substantially falls with rising the Zr content, indicating that the Zr substitution impairs the electrochemical kinetics of the alloys.

It was well known that the high rate discharge ability of a metal hydride electrode is principally dominated by the charge-transfer rate on the surface of an alloy electrode and the hydrogen diffusion capability in the alloy bulk. Hence, it is essential to investigate the charge-transfer rate and the hydrogen diffusion coefficient [6]. The charge-transfer rate on the surface of an alloy electrode is qualitatively evaluated by its electrochemical impedance spectrum (EIS). The EIS of the as-cast and spun $La_{0.75-x}Zr_xMg_{0.25}Ni_{3.2}Co_{0.2}Al_{0.1}$ (x=0-0.2) alloys electrodes are depicted in **Figure 5**. It is found that each EIS spectrum comprises two semicircles corresponding to two different frequency regions. As elucidated by Kuriyama et al. [7], the smaller semicircle in the high frequency region corresponds to the contact resistance between the alloy powder and the conductive material, while the larger semicircle in the low frequency region equates to the charge-transfer resistance on the alloy surface. Hence, the larger the radius of the semicircle in the low frequency region is, the higher the charge-transfer resistance of the alloy electrode will be. It is evident that, with the rising of the spinning rate, the radii of the large semicircles of the $Zr_{0.1}$ alloy

in the low frequency first shrink and then expand, and those of the as-spun (10 m/s) alloys always swell with growing the Zr content. The hydrogen diffusion coefficients in the alloys can be derived by measuring the semilogarithmic curves of anodic current versus working duration of an alloy as depicted in **Figure 6**. Based on the model founded by White et al. [8], the diffusion coefficient (D) of the hydrogen atoms in the bulk of the alloy can be calculated by following formulae:

$$\log i = \log\left(\pm\frac{6FD}{da^2}(C_0 - C_s)\right) - \frac{\pi^2}{2.303}\frac{D}{a^2}t \qquad (1)$$

$$D = -\frac{2.303a^2}{\pi^2}\frac{d\log i}{dt} \qquad (2)$$

In (2), $\frac{d\log i}{dt}$ is the slope of the linear region of **Figure 6**, which can be gained by origin 7.5 software in a walk. The alloy particle radius (a) is supposed to be a=15 μm. Thus, hydrogen diffusion coefficient D can be easily obtained, and the results are also presented in Figure 6. It is evident that with the rising of the spinning rate, the D values of the $Zr_{0.1}$ alloy first mount up and then fall, and those of the as-spun (10 m/s) alloys monotonously drop with rising the Zr content.

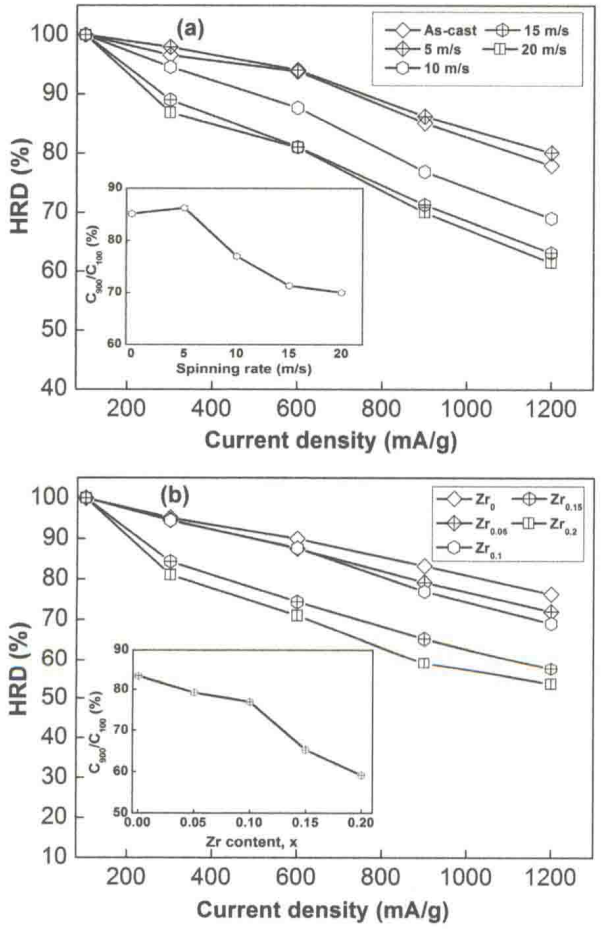

Figure 4. Evolution of the high rate discharge ability (HRD) of the alloys with the discharge current density: (a) $Zr_{0.1}$ alloy, (b) As-spun (10 m/s).

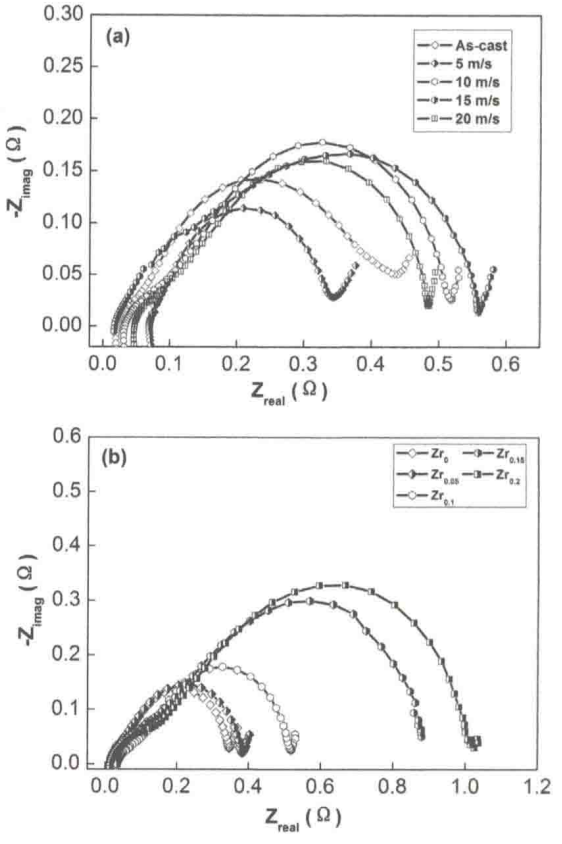

Figure 5. Electrochemical impedance spectra (EIS) of the alloy electrodes: (a) $Zr_{0.1}$ alloy, (b) As spun (10 m/s).

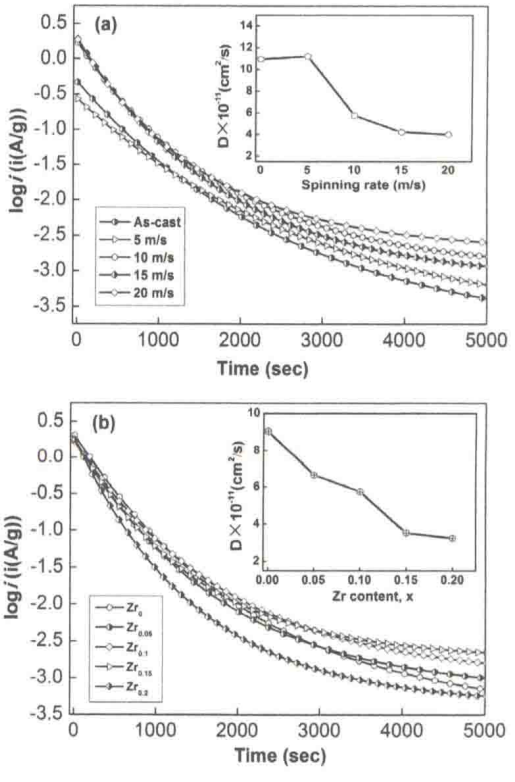

Figure 6. Semilogarithmic curves of anodic current vs. time responses of the alloys: (a) As-spun (10 m/s), (b) $Zr_{0.15}$ alloy.